

JGR Atmospheres

RESEARCH ARTICLE

10.1029/2020JD032641

Key Points:

- TC genesis locations are shifted northward in the BoB during the positive phase of the CIO mode, and it is different from the impact of MJO
- During the positive phase of the CIO mode, convection center moves to the northern BoB, and barotropic energy gain from ISVs nourishes TC genesis
- The shift of TC genesis locations leads to more TC landfalls over the northern BoB

Supporting Information:

- Supporting Information S1

Correspondence to:

L. Zhou,
zhoulei1588@sjtu.edu.cn

Citation:

Li, B., Zhou, L., Wang, C., Gao, C., Qin, J., & Meng, Z. (2020). Modulation of tropical cyclone genesis in the Bay of Bengal by the Central Indian Ocean mode. *Journal of Geophysical Research: Atmospheres*, 125, e2020JD032641.
<https://doi.org/10.1029/2020JD032641>

Received 20 FEB 2020

Accepted 22 MAY 2020

Accepted article online 11 JUN 2020

Modulation of Tropical Cyclone Genesis in the Bay of Bengal by the Central Indian Ocean Mode

Baosheng Li¹ , Lei Zhou^{1,2} , Chunzai Wang^{3,4,5} , Cong Gao¹, Jianhuang Qin¹ , and Ze Meng¹

¹School of Oceanography, Shanghai Jiao Tong University, Shanghai, China, ²Southern Marine Science and Engineering Guangdong Laboratory (Zhuhai), Zhuhai, China, ³State Key Laboratory of Tropical Oceanography, South China Sea Institute of Oceanology, Chinese Academy of Sciences, Guangzhou, China, ⁴Southern Marine Science and Engineering Guangdong Laboratory (Guangzhou), Guangzhou, China, ⁵Innovation Academy of South China Sea Ecology and Environmental Engineering, Chinese Academy of Sciences, Guangzhou, China

Abstract Tropical cyclones (TCs) can be modified by various processes in the multiscale weather and climate system. In this study, the TC genesis locations are found to shift northward in the Bay of Bengal (BoB) due to the intraseasonal central Indian Ocean (CIO) mode. During the positive phase of the CIO mode, convection center moves from the equator to the BoB. Correspondingly, over the BoB, the updraft transports moisture to the mid-troposphere, and the associated convergence and cyclonic vorticity in the lower troposphere are favorable for TC genesis. The diagnoses on eddy kinetic energy budget indicate that the barotropic energy gain from intraseasonal variabilities nourishes TC genesis over the BoB, which is mainly attributable to the horizontal gradient of zonal winds associated with the enhanced low-level convergence and vorticity during the positive CIO mode. During the negative CIO mode, convection is around the equator. The TC genesis locations shift southward, but the modifications are not significant. The impacts of the CIO mode on TC genesis over the BoB are different from the influences of Madden-Julian Oscillation. Hence, the results are expected to contribute to a comprehensive understanding of the relations between TCs and intraseasonal variabilities over the Indian Ocean.

1. Introduction

Tropical cyclone (TC) is one of the most severe natural disasters in the tropics, which has significant impacts on humans and socioeconomic activities. The TC number in the North Indian Ocean (NIO) is relatively small compared with those in the Pacific and the Atlantic. However, due to the high population density on the rim of the NIO, TCs occurring in this region can cause huge casualties and extensive damages. For example, Cyclones Gonu (2007) and Nargis (2008) led to disastrous rainfall and winds to southeastern Asia and the Arabian Peninsula (Kikuchi et al., 2009; Webster, 2008). It has been recognized for a long time that TC genesis can be modified by various natural variabilities, such as El Niño-Southern Oscillation (ENSO) and Indian Ocean Dipole (IOD). Since Atkinson (1977) realized an abnormal TC number in the western North Pacific (WNP) during the 1972 El Niño, a series of work has been conducted on the relationship between ENSO and TCs (e.g., Camargo et al., 2007; Chan, 1985, 2000; Chan & Shi, 1996). In El Niño years, there are usually a southeastward displacement of the mean TC genesis region in the WNP and fewer intense TCs in the Bay of Bengal (BoB; Girishkumar & Ravichandran, 2012; Ng & Chan, 2012) due to the increase of the low-level cyclonic shear corresponding to the shift of convection and the deepening of the monsoon trough (Chia & Ropelewski, 2002; Wang & Chan, 2002). The IOD impact on the interannual variabilities of TC genesis locations was also examined. It was concluded that more TCs occurred in the northern BoB ($15^{\circ}\text{--}20^{\circ}\text{N}$ and $85^{\circ}\text{--}95^{\circ}\text{E}$) as the warm sea surface temperature (SST) anomalies strengthen convection and cause the cyclonic circulation at the lower troposphere during the negative phase of IOD (Mahala et al., 2015; Yuan & Cao, 2013).

In the Indian Ocean, intraseasonal variabilities (ISVs) are pronounced and have distinct influences on TC genesis. A major component of ISVs is the Madden-Julian Oscillation (MJO; Zhang, 2005), which is usually represented by the Real-time Multivariate MJO (RMM) index developed by Wheeler and Hendon (2004). The influences of MJO on TC genesis in the Indian Ocean were analyzed by Krishnamohan et al. (2012). They concluded that TCs preferred to occur during the convective phase of MJO as westerlies at 850 hPa

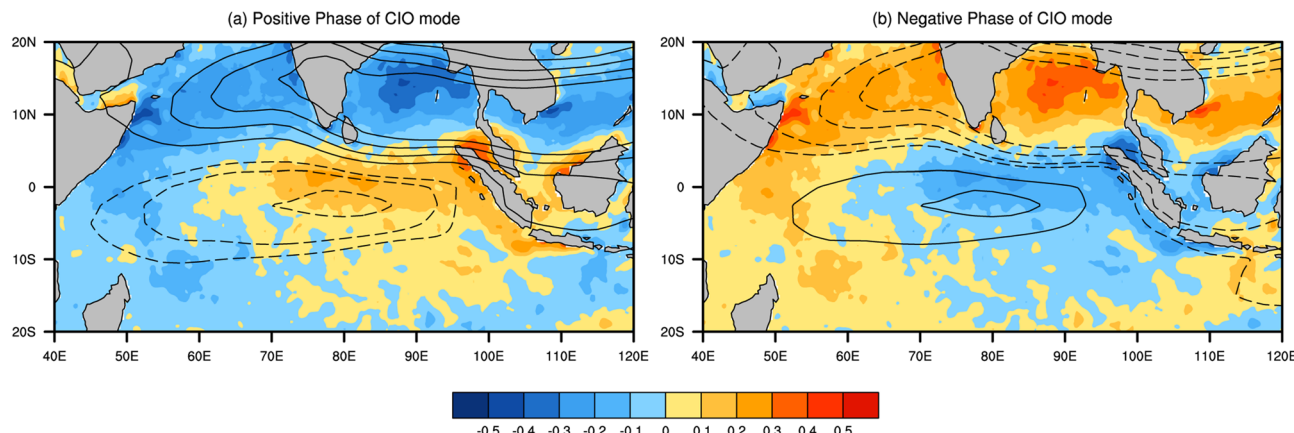


Figure 1. The pattern of the (a) positive and (b) negative phase of the CIO mode. Reddish (bluish) color denotes the positive (negative) anomaly of the SST mode. Solid (dashed) contours denote the positive (negative) anomaly of the zonal wind mode.

associated with MJO create strong cyclonic vorticity, which was found to be related to 44 TCs out of the total 54 TCs within 0–15°N and 60–100°E. Enhanced convection over the Maritime Continent during MJO is favorable for TC genesis over the NIO, since it creates strong cyclonic vorticity in the lower troposphere along with the small vertical wind shear (Bessafi & Wheeler, 2006; Girishkumar et al., 2015; Ho et al., 2006; Krishnamohan et al., 2012).

However, there are other ISVs that do not belong to MJO. Recently, a central Indian Ocean (CIO) mode was found by Zhou et al. (2017a), which had a high correlation with intraseasonal rainfall in the Indian monsoon region. The CIO mode is defined as the first combined empirical orthogonal function (EOF) mode of intraseasonal SST anomalies and intraseasonal zonal wind anomalies at 850 hPa. As shown in Figure 1a, during the positive phase of the CIO mode, the positive SST anomaly of the combined EOF mode captures warm intraseasonal SST anomalies in the equatorial Indian Ocean. Correspondingly, the negative wind anomaly denoting the equatorial easterlies and the positive wind anomaly denoting the westerlies from the Arabian Sea to the South China Sea indicate an anticyclonic gyre between the equatorial Indian Ocean and tropics. The negative phase of the CIO mode is defined as the opposite to the positive one (Figure 1b). The robustness of this mode was tested by perturbing the regions for the EOF analysis and by using different reanalysis products (Zhou et al., 2017a, 2017b, 2018). The warm intraseasonal SST anomalies and the associated anticyclone are the key features of the positive phase of the CIO mode. Due to the strong anticyclone over the warm SST, the vertical structure of the CIO mode is more like a barotropic structure. As a result, the barotropic energy conversion is the major energy source for the CIO mode (Zhou et al., 2017a, 2017b). In contrast, the baroclinic structure for MJO had been widely recognized (e.g., Adames & Wallace, 2014), and the baroclinic energy conversion is dominant for MJO (Zhou et al., 2012). In addition, the CIO mode index and the RMM2 for MJO (Wheeler & Hendon, 2004) are shown in Figure 2. Since negative RMM2 indicates deep convection occurs over the open Indian Ocean, for the cleanliness of the figure, only RMM2 is shown in Figure 2. However, the relation between RMM1 and the CIO mode index is similar. Correlation coefficient of daily CIO mode index with daily RMM2 (RMM1) is 0.35 (0.38) from 1982 to 2017. The correlation coefficients are not statistically significant at a 99% confidence level. Moreover, all peaks in CIO mode index, which are larger than its standard deviation (STD) and denote significant deep convection events, are marked with red dots in Figure 2. The significantly large RMM2 peaks are marked with blue dots. From 1982–2017, the CIO mode peaks 396 times, whereas RMM2 (RMM1) reaches maximum 416 (436) times. The occurring times for pronounced deep convection events associated with the CIO mode and MJO are mostly inconsistent. Overall, the CIO mode is largely independent from the MJO.

Therefore, an examination on the impact of the CIO mode on TC genesis over the NIO is expected to provide new information on the relation between ISVs and TCs in the Indian Ocean, which is the motivation of this study. For the rest of this paper, data and methods are introduced in Section 2. TC genesis in different phases of the CIO mode are discussed in Section 3. Finally, conclusions and discussion are presented in Section 4.

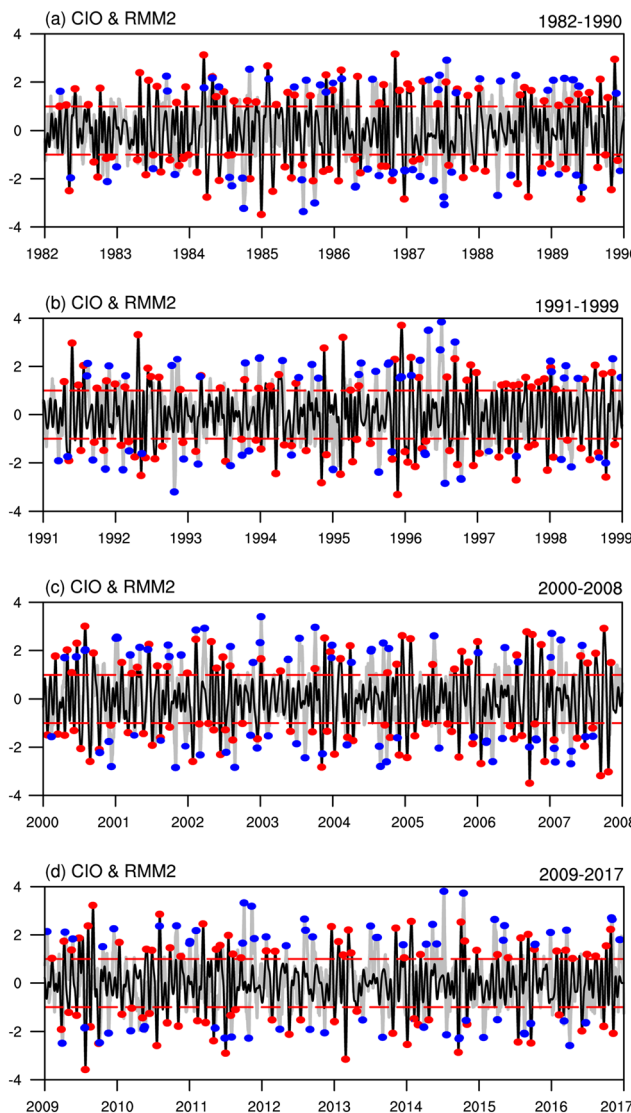


Figure 2. The CIO mode index (black line) and RMM2 (gray line) during (a) 1982–1990; (b) 1991–1999; (c) 2000–2008; (d) 2009–2017. The red dashed lines denote the thresholds (one standard deviation) for the positive and negative phases of the CIO mode. The significant CIO mode peaks marked with red circles and the peak of RMM2 with blue circles. Correlation coefficient of daily CIO mode index and RMM2 (RMM1) is 0.35 (0.38) from 1982 to 2017. RMM1 is not shown in this figure.

scale. However, for the completeness of decomposition, all components are retained in following analyses. Thus, the ISV scale and the slow variabilities (slower than 100 days) are considered as the background components. The statistical significance is assessed via the two-tailed Student's *t* test. The effective degree of freedom is determined following Pyper and Peterman (1998).

3. Results

The TC genesis locations during the positive and negative phases of the CIO mode from 1982 to 2017 are shown in Figure 3a. There are 60 TCs (the sum of blue and red dots in Figure 3a) generating along with the significant CIO mode, which account for 32% of total TCs over the NIO. In the positive phase, 29 TCs generate in the NIO, 20 out of which occur to the north of 10°N (red dots in Figure 3a). Only eight TCs

2. Data and Methods

TC genesis positions over the NIO from 1982 to 2017 are obtained from the Joint Typhoon Warning Center (JTWC) tropical cyclone track data. Since a climate shift occurred in the late 1970s, the period focused in this study starts from 1982, and the possible modifications due to climate shift are not considered. In this study, only TCs that reach the tropical storm intensity (the maximum sustained 10-meter wind speed is larger than 17.2 m s⁻¹) are considered. Daily variables, such as horizontal winds, specific humidity, and vertical velocity, are obtained from ERA-Interim, a global atmospheric reanalysis produced by the European Centre for Medium-Range Weather Forecasts (ECMWF; Dee et al., 2011). The horizontal resolution is 1.5° latitude × 1.5° longitude. Daily atmospheric variables from the National Centers for Environmental Prediction—National Center for Atmospheric Research (NCEP-NCAR) reanalysis (Kalnay et al., 1996) are also used to verify the robustness of the results (not shown). The SST data for 1982–2017 are obtained from the 1/4° daily NOAA Optimum Interpolation SST (Reynolds et al., 2007). All intraseasonal variabilities are obtained with a 20–100-day bandpass Butterworth filter.

The positive (negative) CIO mode phases are defined when the daily CIO mode index is larger (smaller) than its STD, so that convection associated with the CIO mode is pronounced in the Indian Ocean. The following statistics of TC genesis numbers and the composite analysis on environmental variables are fulfilled for the positive and negative CIO phases, respectively. Since the CIO mode is a persistent mode in the Indian Ocean (Zhou et al., 2017b), all seasons in the 36 years (from 1982 to 2017) are examined.

The barotropic energy conversion (BT) is examined in previous studies on the modulation of TCs (Hong et al., 2018; Maloney & Hartmann, 2001; Sobel & Maloney, 2000). BT is explicitly calculated as

$$BT = -u'v'\frac{\partial \bar{u}}{\partial y} - u'v'\frac{\partial \bar{v}}{\partial x} - u'^2\frac{\partial \bar{u}}{\partial x} - v'^2\frac{\partial \bar{v}}{\partial y}, \quad (1)$$

where u and v are zonal and meridional wind velocities, respectively. The eddy component of each variable is obtained using a high-pass filtering with a cutoff period of 20 days, and it is denoted with a prime. The background component of each variable is obtained with a 20-day low-pass filtering, and it is denoted with an overbar. The background components consist of both ISVs and all slower variabilities. Generally, it is assumed that energy conversion only efficiently happens between two adjacent scales, for example, between the eddy scale and the ISV

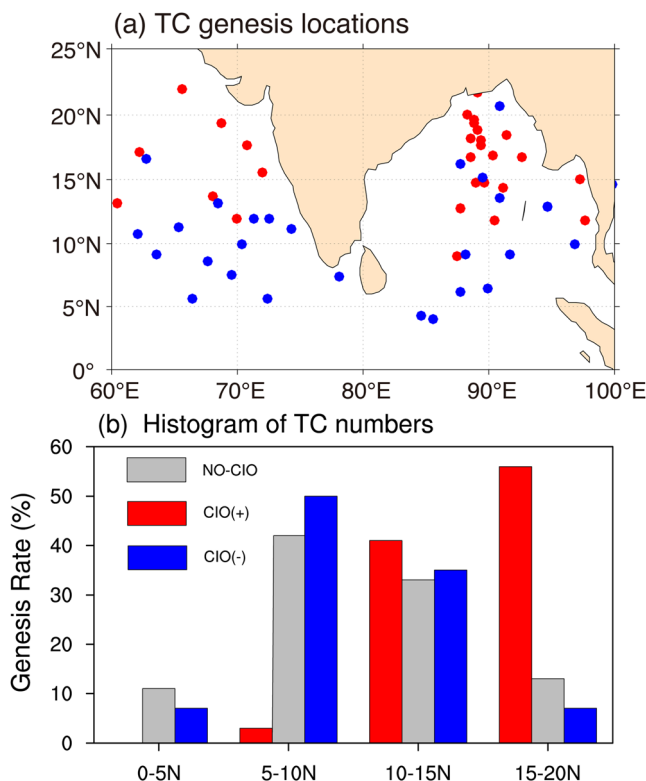


Figure 3. (a) TC genesis locations during the positive phase of the CIO mode (red circles) and the negative phase of the CIO mode (blue circles) from 1982 to 2017. (b) Histogram of the TC numbers within 5° latitude bins. The red bars (blue bars) denote TCs during the positive (negative) phase of the CIO mode and the gray bars denote TCs without the CIO mode.

occur in the Arabian Sea (AS). In contrast, during the negative phase of the CIO mode, 31 TCs generate, and the locations spread the whole NIO, as shown with the blue dots in Figure 3a. The TC genesis locations show a significant difference between the positive and negative phases of the CIO mode, although the difference in the total TC number is not significant. The mean latitude of TC genesis locations is 16.3°N (10.6°N) during the positive (negative) phase of the CIO mode, whose confidence interval at 99% confidence level is 15.7–17°N (8.9–12.4°N). The northward shift of TC genesis is significantly different from the normal condition with (9.7°N, 11.3°N) at a 99% confidence level using the Student's *t* test. The histogram of the TC genesis numbers within 5° latitude bins is shown in Figure 3b, and the distributions of TC genesis locations at each 5° × 5° box are presented in the supporting information Figure S1. During the positive phase of the CIO mode, over half TCs (17 TCs) generate to the north of 15°N. Another 41% (11 TCs) generate between 10°N and 15°N. Merely 3% (1 TC) occur to the south of 10°N. In contrast, when the CIO mode is not active (gray bars in Figure 3b), over 50% TCs generate within 5–10°N and the percentage decreases with the latitude increases. Less than 15% TCs generate in the northern BoB (between 15°N and 20°N) when the CIO mode is not active. During the negative phase of the CIO mode, TC genesis has a similar distribution with that when the CIO mode is not active. A total of 14 (48%) and 10 (34%) TCs generate within 5–10°N and 10–15°N, respectively (blue bars in Figure 3b). Similarly, only 10% TCs occur in the northern BoB. Thus, the negative phase of the CIO mode, comparing with the normal condition, has no significant impacts on modifying TC genesis locations.

It is well-known that TC genesis depends on key environmental factors, such as low-level vorticity, updraft, and humidity in the mid-troposphere (Emanuel & Nolan, 2004; Gray, 1979). Given that the climatological environment is the basis for TC genesis, the climatology is presented in Figure S2. The composite anomalies for these factors during the positive phase of the CIO mode are shown in Figure 4. The vorticity anomalies are positive over the northern BoB, with a maximum of about $6 \times 10^{-6} \text{ s}^{-1}$ between 15°N and 20°N during the positive phase of the CIO mode (Figure 4a). In addition, there are convergence in the lower troposphere over the northern BoB (Figure 4b), leading to strong vertical velocity at the midlevel (Figure 4c). The strong vertical velocity usually has a high correlation with the TC frequency in all ocean basins (Zhao & Held, 2012). As a result, the mid-troposphere (500 hPa) is humidified (Figure 4d). Hack and Schubert (1986) revealed that the Rossby radius of deformation decreases with increasing vorticity in a nonlinear idealized model. The reduced scale further led to efficient conversion from latent heat release to rotational motion. It suggests that latent heat release in the midlevel tends to reinforce low-level vorticity. In contrast, negative vorticity and divergence occur from the southern BoB to the equator (to the south of 10°N). There are downdraft and dry anomalies in the mid-troposphere, which are prone to suppress TC genesis. It further leads the TC genesis locations to shift to the northern BoB. Therefore, the modulation on the atmospheric environment by the positive phase of the CIO mode is beneficial to TC genesis in the northern BoB.

During the negative phase of the CIO mode, the composite distributions of vorticity, divergence, vertical velocity, and specific humidity are shown in Figure 5. Generally, the patterns in Figure 5 are similar to those in Figure 4 but with opposite signs. The favorable environment for TC genesis moves near the equator, which is in agreement with deep convection center residing in the equatorial Indian Ocean during the negative CIO mode. Although the circulation near the equator is adjusted, a few more TCs generate to the south of 15°N (blue bars in Figure 3b). Since the Coriolis force is too small, almost no TCs generate near the equator. As a result, comparing with the normal condition, TC genesis locations are not significantly affected during the negative phase of the CIO mode.

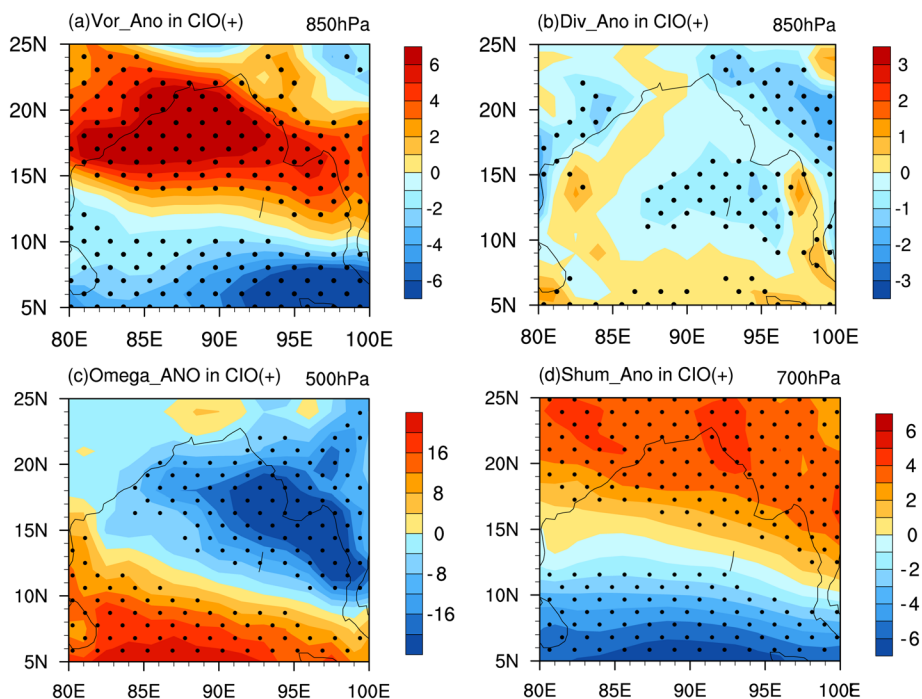


Figure 4. The composite anomalies during the positive phase of the CIO mode from 1982 to 2017: (a) vorticity anomalies (10^{-6} s^{-1}) at 850 hPa; (b) divergence anomalies (10^{-6} s^{-1}) at 850 hPa; (c) vertical velocity anomalies in an isobaric coordinate ($\omega = dp/dt; 10^{-3} \text{ pa s}^{-1}$) at 500 hPa; (d) specific humidity anomalies ($10^{-4} \text{ kg kg}^{-1}$) at 700 hPa. The dotted areas indicate the composite are significantly different from zero at a 99% confidence level.

Furthermore, warm SST anomalies are often needed for TC activities (Emanuel, 1986; Schade & Emanuel, 1999; Zhang et al., 2016). However, over the BoB, SSTs are warm ($\approx 32^{\circ}\text{C}$) enough to support TCs (Figure S3). Generally, a weak vertical wind shear is helpful for maintaining the warm core. The vertical wind shear has a same distribution but an opposite sign between the positive and negative phases of the CIO mode (Figure S4). Although the directions of the wind shears are different, the magnitudes of the vertical wind shears are comparable, which are unfavorable for TC genesis in both phases of the CIO mode. Therefore, the SST anomalies and vertical wind shear are not key variables in the relation between TCs and the CIO mode. Overall, it is shown that the TC genesis is mainly modified by the CIO mode from its significant impacts on various atmospheric properties. During the positive phase of the CIO mode, the environmental conditions are favorable for TC genesis in the northern BoB.

The formation of TCs requires energy from the environment. Large eddy kinetic energy (EKE) can provide “seed” disturbances in the low level that are usually a precursor for TC genesis (e.g., Bracken & Bosart, 2000; Lau & Lau, 1992; Zehr, 1992). For example, Maloney and Hartmann (2001) diagnosed the EKE associated with MJO and concluded that TC genesis increased due to the barotropic energy conversion during the active phase of MJO. Similar conclusions were drawn for the MJO impacts on TC genesis over the western North Pacific (WNP; Hong et al., 2018; Maloney & Dickinson, 2003). On interannual timescales, ENSO leaves footprints on TCs via modulating the barotropic energy conversion (Sobel & Maloney, 2000; Zhan et al., 2011). Furthermore, composite barotropic energy conversion in Equation 1 for the positive phase of the CIO mode is shown in Figure 6a. The maximum center of BT over the northeastern BoB ($88\text{--}95^{\circ}\text{E}$ and $15\text{--}20^{\circ}\text{N}$) supplies energy to TC genesis, which corresponds to the TC genesis locations. In addition, from 15°N to the equator, the composite BT decreases with latitude, and thus, the weak energy leads to fewer TC genesis to the south of 15°N . Conversely, during the negative phase of the CIO mode, the composite BT over the northern BoB is smaller than that during the positive phase by about 80% (Figure 6b), which is consistent with the fact that fewer TCs generate over the northern BoB in the negative phase of the CIO mode. Within the region between 5°N and 10°N , the composite BT is larger than that in the northern BoB. However, due to the small planetary vorticity at low latitudes, the number of TC formation in this area does not increase significantly.

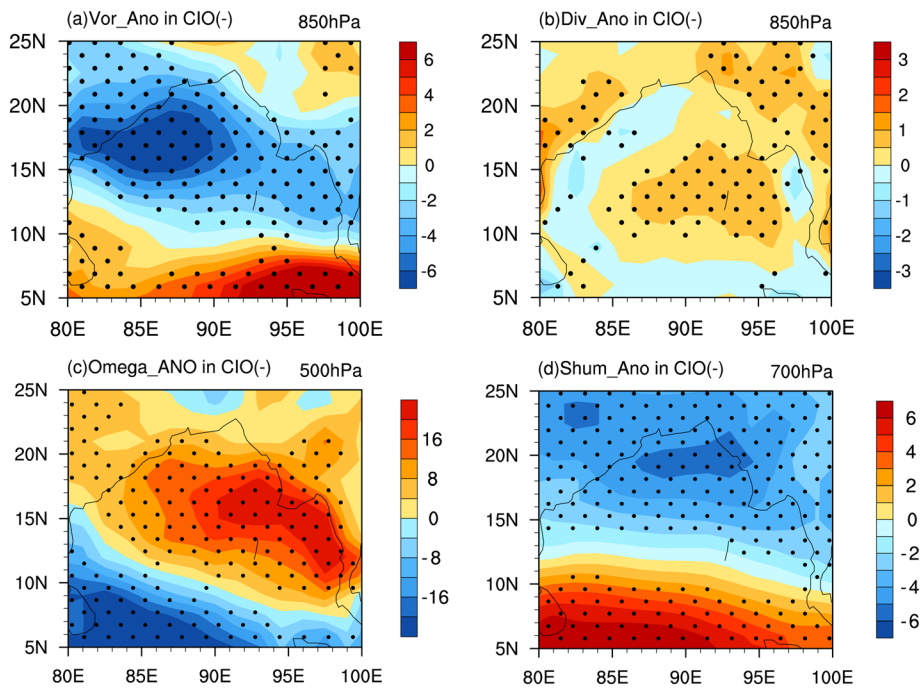


Figure 5. Same as Figure 4 but during the negative phase of the CIO mode.

All components of BT in Equation 1 during the positive phase of the CIO mode are shown in Figure 7. Large $-u'v\frac{\partial\bar{u}}{\partial y}$ locates in the northern BoB in excess of $1.2 \text{ m}^2 \text{ s}^{-2}$ (Figure 7a), which is similar to the distribution of BT. Negative $-u'v\frac{\partial\bar{v}}{\partial x}$ reduces BT in the northern BoB, but its center locates around 85°E (Figure 7b). Since TC genesis concentrates around 90°E , the impact of $-u'v\frac{\partial\bar{v}}{\partial x}$ is small in this region. However, $-u'^2\frac{\partial\bar{u}}{\partial x}$ contributes similar amount of energy as $-u'v\frac{\partial\bar{u}}{\partial y}$ does in the northeastern BoB within $15\text{--}20^\circ\text{N}$ and $88\text{--}95^\circ\text{E}$ (Figure 7c). In the same region in Figure 7d, $-v'^2\frac{\partial\bar{v}}{\partial y}$ has a negative contribution to BT. Positive $-v'^2\frac{\partial\bar{v}}{\partial y}$ is

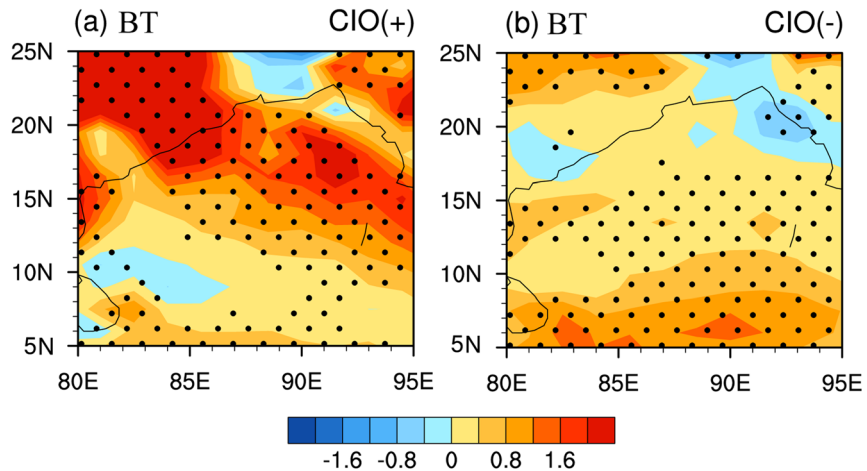


Figure 6. The composite barotropic energy conversion term ($\text{m}^2 \text{ s}^{-3}$) in the EKE budget during the (a) positive and (b) negative phase of the CIO mode from 1982 to 2017. The dotted areas indicate the composites are significantly different from zero at a 99% confidence level.

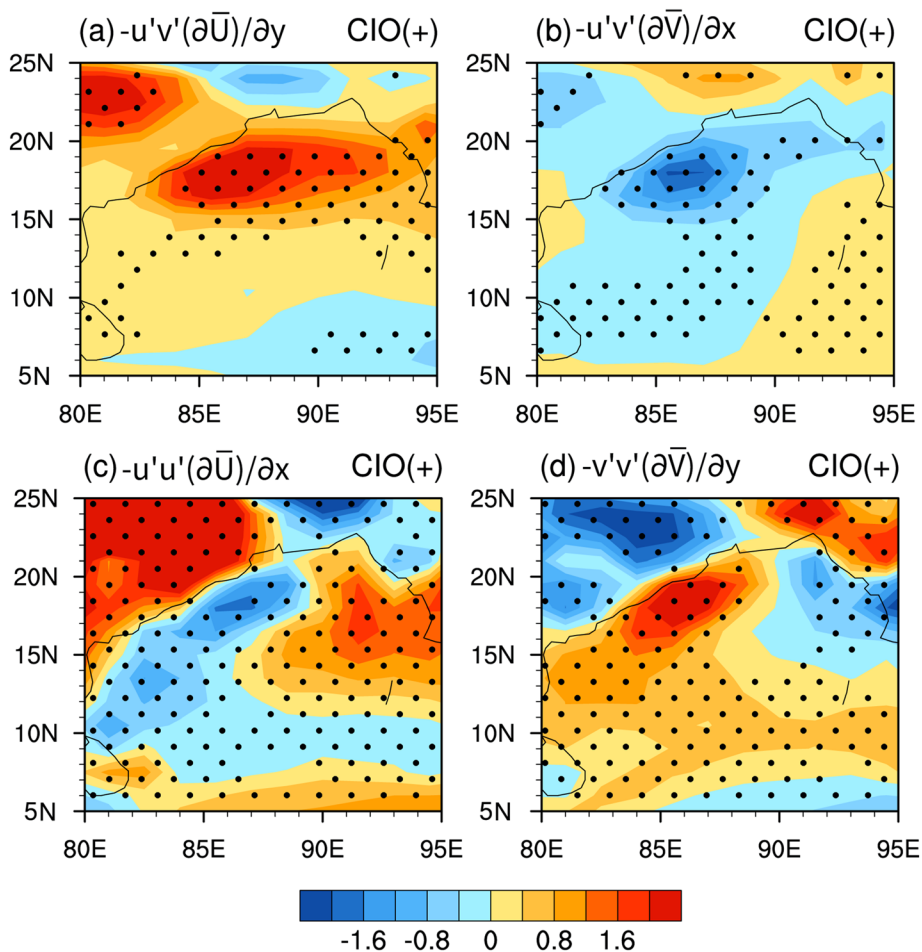


Figure 7. The composite barotropic energy conversion terms of (a) $-u'v'\frac{\partial\bar{U}}{\partial y}$, (b) $-u'v'\frac{\partial\bar{V}}{\partial x}$, (c) $-u'^2\frac{\partial\bar{U}}{\partial x}$, (d) $-v'^2\frac{\partial\bar{V}}{\partial y}$ during the positive phase of the CIO mode from 1982 to 2017. The unit for all terms is $\text{m}^2 \text{s}^{-3}$. The dotted areas indicate the composites are significantly different from zero at a 99% confidence level.

within 15–20°N and 85–88°E, which is not along with the majority of TC genesis location. In contrast, components of BT during the negative phase of the CIO mode are shown in Figure 8. Large values of all terms occur to the south of 10°N. The term $-u'^2\frac{\partial\bar{U}}{\partial x}$ still dominates in BT, and its maximum center locates within 5–10°N and 88–95°E (Figure 8c). The term $-u'v'\frac{\partial\bar{U}}{\partial y}$ supplies energy to BT in the region of 5–10°N and 80–85°E, as shown in Figure 8a. Thereby, BT over the northern BoB is dominated by $-u'v'\frac{\partial\bar{U}}{\partial y}$ and $-u'^2\frac{\partial\bar{U}}{\partial x}$ during the positive phase of the CIO mode, which is caused by eddy interactions with zonal gradients and meridional gradients of background zonal winds. The terms of $-u'v'\frac{\partial\bar{U}}{\partial y}$ and $-u'^2\frac{\partial\bar{U}}{\partial x}$ are also the dominant components of BT for the negative phase of the CIO mode. But the locations are close to the equator; thus, TC genesis locations are not significantly modified.

Since the composites of u' and v' have similar distributions and magnitudes in the positive and negative phases of the CIO mode (Figure S5), background wind shears explain the differences between different BT components. The zonal and meridional gradients of \bar{u} are displayed in Figure 9. In Figure 9a, pronounced negative $\frac{\partial\bar{U}}{\partial y}$ is located over the northern BoB, which corresponds to large $-u'v'\frac{\partial\bar{U}}{\partial y}$ for the positive phase of the CIO mode. Moreover, negative $\frac{\partial\bar{U}}{\partial x}$ over the northeastern BoB leads to large $-u'^2\frac{\partial\bar{U}}{\partial x}$ in this region during

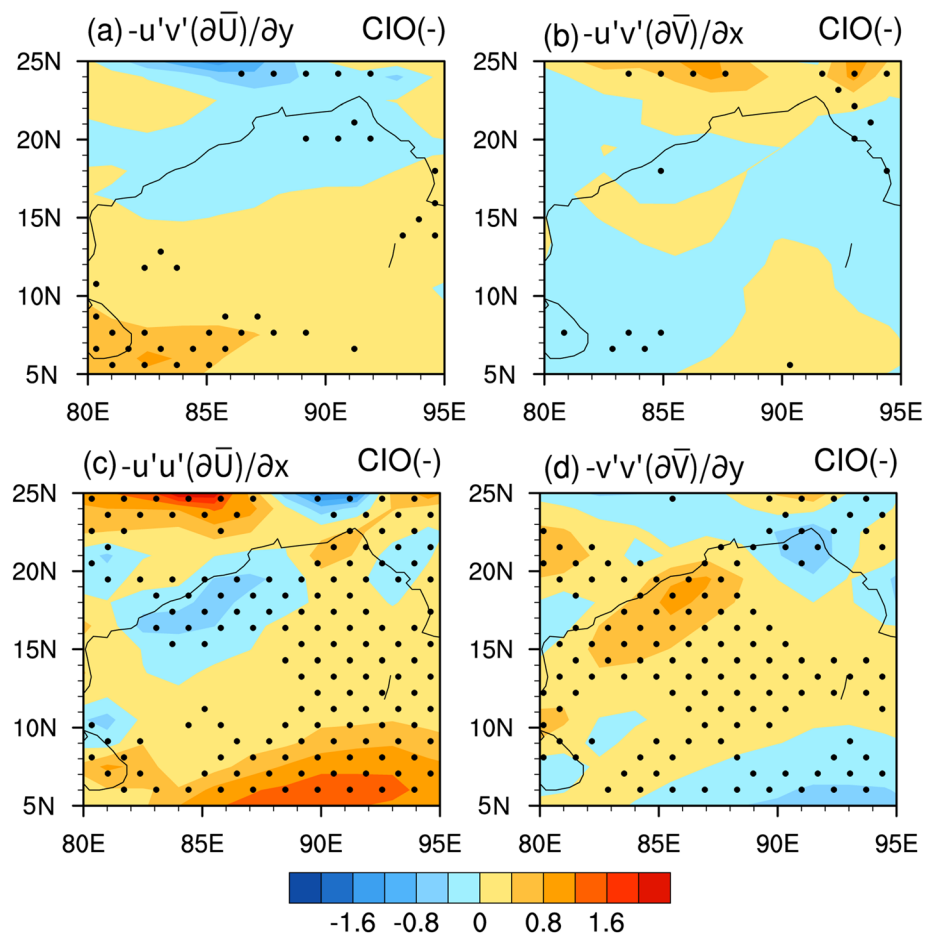


Figure 8. Same as Figure 7 but during the negative phase of the CIO mode.

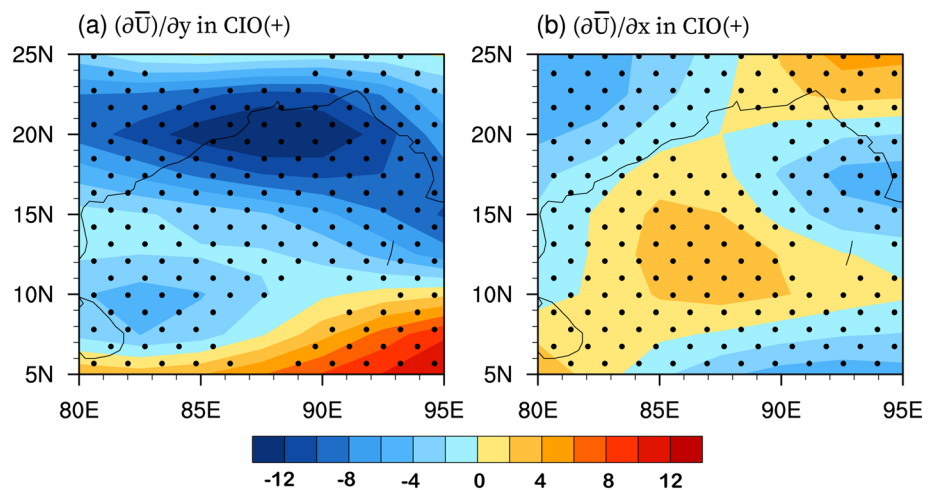


Figure 9. The composite (a) $\frac{\partial \bar{U}}{\partial y}$ and (b) $\frac{\partial \bar{U}}{\partial x}$ at 850 hPa (colors; 10^{-6} s^{-1}) during the positive phase of the CIO mode from 1982 to 2017. The dotted areas indicate the composites are significantly different from zero at a 99% confidence level.

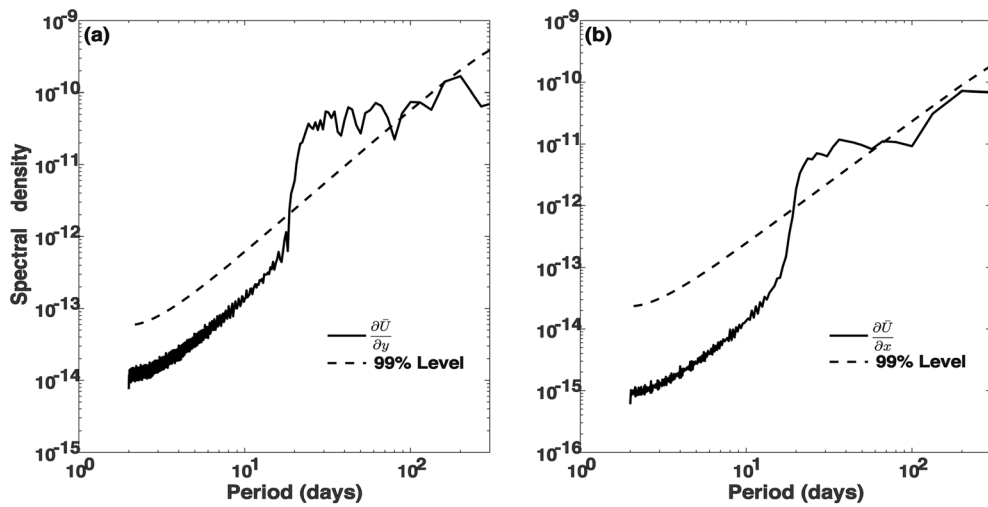


Figure 10. Power spectra for (a) $\frac{\partial \bar{U}}{\partial y}$ and (b) $\frac{\partial \bar{U}}{\partial x}$ averaged over the BoB ($5\text{--}25^\circ\text{N}$; $80\text{--}95^\circ\text{E}$) are shown with solid lines, and the 99% confidence levels are presented with the dashed lines. The unit for the left axis is s^{-2} .

the positive phase of the CIO mode (Figure 9b), which is consistent with TC genesis shown in Figure 3a (red dots).

Since the background zonal wind \bar{u} is composed of ISVs and all variabilities with longer timescales, the power spectra of $\frac{\partial \bar{u}}{\partial x}$ and $\frac{\partial \bar{u}}{\partial y}$ averaged within the northern BoB are analyzed to identify the major frequencies. As shown in Figures 10a and 10b, respectively, the spectra for $\frac{\partial \bar{u}}{\partial y}$ are significant between 20–80 days, and the spectra for $\frac{\partial \bar{u}}{\partial x}$ are significant between 20 and 60 days. The spectra with a period longer than 100 days in $\frac{\partial \bar{u}}{\partial x}$ and $\frac{\partial \bar{u}}{\partial y}$ are not significant. It can be concluded that the meridional and zonal gradients of \bar{u} ($\frac{\partial \bar{u}}{\partial y}$ and $\frac{\partial \bar{u}}{\partial x}$) are dominated by ISVs. As shown in Figure 9a, $\frac{\partial \bar{u}}{\partial y}$ is negative in the northern BoB during the positive phase of the CIO mode, which implies a positive vorticity ($\zeta = \frac{\partial v}{\partial x} - \frac{\partial u}{\partial y}$) on intraseasonal timescales. In addition, $\frac{\partial \bar{u}}{\partial x}$ is positive in the northern BoB as shown in Figure 9b, which indicates low-level convergence. Therefore,

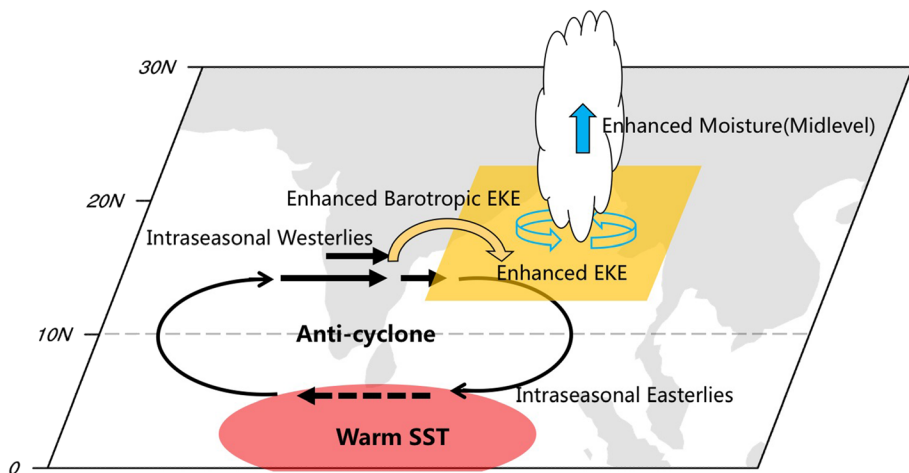


Figure 11. Sketch for the processes during the positive phase of the CIO mode.

intraseasonal components in $\frac{\partial \bar{u}}{\partial y}$ and $\frac{\partial \bar{u}}{\partial x}$ are consistent with the enhanced cyclonic vorticity and convergence in the lower troposphere, as shown in Figures 4a and 4b. The large horizontal gradients associated with the positive phase of the CIO mode trigger the barotropic energy conversion and supply EKE to TC genesis over the northern BoB.

4. Conclusions

TC genesis over the NIO can be modified by ISVs. The influences of MJO, as a major component of ISVs, were discussed by Bessafi and Wheeler (2006), Girishkumar and Ravichandran (2012), and Krishnamohan et al. (2012). The CIO mode was proposed as another intraseasonal process over the Indian Ocean (Zhou et al., 2017a). The CIO mode has distinct properties and dynamics compared to the MJO (Zhou et al., 2017a, 2017b), and the days with the active CIO mode are also different from those with active MJO. In this study, the impacts of the CIO mode, especially the positive phase of the CIO mode, on TC genesis over the NIO are examined. The results show that the TC genesis locations have a clear northward shift from the tropical Indian Ocean to the northern BoB during the positive phase of the CIO mode. As illustrated in Figure 11, the dynamical and thermodynamical environments modified by the positive CIO mode are favorable for TC genesis over the northern BoB, including the positive vorticity and convergence in the lower troposphere, strong updraft, and enhanced humidity in the mid-troposphere. Moreover, the distinguished horizontal gradients of background zonal winds ($\frac{\partial \bar{u}}{\partial y}$ and $\frac{\partial \bar{u}}{\partial x}$), accompanied with the vorticity and convergence, lead to barotropic energy conversion and provide EKE to TC genesis. During the negative phase of the CIO mode, convection center is near the equator. Atmospheric and oceanic environments are favorable for TC genesis, such as large vorticity and warm SST anomalies. But they are close to the equator. As a result, TC genesis is not significantly enhanced near the equator. Correspondingly, the TC genesis locations spread over the NIO, which are similar to the normal situation.

Due to the northward shift of the TC genesis locations during the positive phase of the CIO mode, more TCs tend to make landfalls on the northern rim of the BoB and may cause dramatic damages in the heavily populated region. A total of 22 (76%) TCs hit the land during the positive phase of the CIO mode. Without the impacts of the CIO mode, 67% (84 out of 125) TCs make landfall over the NIO. The shift of the TC genesis locations also leads to the shift of landfall positions. There are 22 TCs making landfall to the north of 10°N, which account for 76% of 29 TCs generating during the positive phase of the CIO mode. In contrast, out of 125 TCs beyond the period of the CIO mode, 34% make landfalls to the north of 10°N.

Nowadays, the importance of a multiscale “seamless” climate system has been well recognized (Brunet et al., 2010; Hurrell et al., 2009; Palmer et al., 2008; Zhang, 2013). Except for the influences from ISVs, TC genesis in the NIO is also subject to other processes in the climate system, such as ENSO and IOD (Girishkumar et al., 2015; Mahala et al., 2015; Ng & Chan, 2012). Meanwhile, the CIO mode also has a clear interannual variability, which is partly related to ENSO and IOD (Zhou et al., 2017b). In a “seamless” framework, more work is needed to explore the joint impacts of various climate processes on TC genesis in the Indian Ocean.

Data Availability Statement

The reanalysis products are provided by the ECWMF and NOAA/ESRL PSD, which can be obtained from their websites (<https://apps.ecmwf.int/datasets/> and <https://www.esrl.noaa.gov/psd/>, respectively). The tropical cyclone track data for this paper are publicly available from the Official U.S. Navy Website (<https://www.metoc.navy.mil/jtvc/jtvc.html>).

References

- Adames, Á. F., & Wallace, J. M. (2014). Three-dimensional structure and evolution of the MJO and its relation to the mean flow. *Journal of the Atmospheric Sciences*, 71(6), 2007–2026. <https://doi.org/10.1175/JAS-D-13-0254.1>
- Atkinson, G. (1977). Proposed system for near real time monitoring of global tropical circulation and weather patterns. Paper presented at preprints, 11th tech. Conf. on Hurricanes and Tropical Meteorology, Miami Beach, FL, Amer. Meteor. Soc.
- Bessafi, M., & Wheeler, M. C. (2006). Modulation of south Indian Ocean tropical cyclones by the Madden-Julian oscillation and convectively coupled equatorial waves. *Monthly Weather Review*, 134(2), 638–656. <https://doi.org/10.1175/MWR3087.1>

Acknowledgments

This work is supported by grants from the Strategic Priority Research Program of Chinese Academy of Sciences (Grant No. XDB42000000), the National Natural Science Foundation of China (41731173, 41690121, 41690120, 41530961, 41621064), the National Key Research and Development Program of China (2019YFA0606701), the IPOVAR Project (GASI-IPOVAI-01-02, GASI-IPOVAI-02), the Key Special Project for Introduced Talents Team of Southern Marine Science and Engineering Guangdong Laboratory (Guangzhou) (GML2019ZD0306), the Pioneer Hundred Talents Program of the Chinese Academy of Sciences, and the Leading Talents of Guangdong Province Program.

- Bracken, W. E., & Bosart, L. F. (2000). The role of synoptic-scale flow during tropical cyclogenesis over the North Atlantic Ocean. *Monthly Weather Review*, 128(2), 353–376. [https://doi.org/10.1175/1520-0493\(2000\)128%3C0353:TROSSF%3E2.0.CO;2](https://doi.org/10.1175/1520-0493(2000)128%3C0353:TROSSF%3E2.0.CO;2)
- Brunet, G., Shapiro, M., Hoskins, B., Moncrieff, M., Dole, R., Kiladis, G. N., et al. (2010). Collaboration of the weather and climate communities to advance subseasonal-to-seasonal prediction. *Bulletin of the American Meteorological Society*, 91(10), 1397–1406. <https://doi.org/10.1175/2010BAMS3013.1>
- Camargo, S. J., Emanuel, K. A., & Sobel, A. H. (2007). Use of a genesis potential index to diagnose ENSO effects on tropical cyclone genesis. *Journal of Climate*, 20(19), 4819–4834. <https://doi.org/10.1175/JCLI4282.1>
- Chan, J. C. L. (1985). Tropical cyclone activity in the Northwest Pacific in relation to the El Niño/southern oscillation phenomenon. *Monthly Weather Review*, 113(4), 599–606. [https://doi.org/10.1175/1520-0493\(1985\)113%3C0599:TCAITN%3E2.0.CO;2](https://doi.org/10.1175/1520-0493(1985)113%3C0599:TCAITN%3E2.0.CO;2)
- Chan, J. C. L. (2000). Tropical cyclone activity over the Western North Pacific associated with El Niño and La Niña events. *Journal of Climate*, 13(16), 2960–2972. [https://doi.org/10.1175/1520-0442\(2000\)013%3C2960:TCAUTW%3E2.0.CO;2](https://doi.org/10.1175/1520-0442(2000)013%3C2960:TCAUTW%3E2.0.CO;2)
- Chan, J. C. L., & Shi, J. (1996). Long-term trends and interannual variability in tropical cyclone activity over the western North Pacific. *Geophysical Research Letters*, 23(20), 2765–2767. <https://doi.org/10.1029/96GL02637>
- Chia, H. H., & Ropelewski, C. F. (2002). The interannual variability in the genesis location of tropical cyclones in the Northwest Pacific. *Journal of Climate*, 15(20), 2934–2944. [https://doi.org/10.1175/1520-0442\(2002\)015%3C2934:TIVITG%3E2.0.CO;2](https://doi.org/10.1175/1520-0442(2002)015%3C2934:TIVITG%3E2.0.CO;2)
- Dee, D. P., Uppala, S. M., Simmons, A. J., Berrisford, P., Poli, P., Kobayashi, S., et al. (2011). The ERA-interim reanalysis: Configuration and performance of the data assimilation system. *Quarterly Journal of the Royal Meteorological Society*, 137(656), 553–597. <https://doi.org/10.1002/qj.828>
- Emanuel, K., & Nolan, D. S. (2004). Tropical cyclone activity and the global climate system. Paper presented at 26th Conference on Hurricanes and Tropical Meteorology.
- Emanuel, K. A. (1986). An air-sea interaction theory for tropical cyclones. Part I: Steady-state maintenance. *Journal of the Atmospheric Sciences*, 43(6), 585–605. [https://doi.org/10.1175/1520-0469\(1986\)043%3C0585:aasitf%3E2.0.co;2](https://doi.org/10.1175/1520-0469(1986)043%3C0585:aasitf%3E2.0.co;2)
- Girishkumar, M. S., & Ravichandran, M. (2012). The influences of ENSO on tropical cyclone activity in the Bay of Bengal during October–December. *Journal of Geophysical Research*, 117, C02033. <https://doi.org/10.1029/2011JC007417>
- Girishkumar, M. S., Suprit, K., Vishnu, S., Prakash, V. T., & Ravichandran, M. (2015). The role of ENSO and MJO on rapid intensification of tropical cyclones in the Bay of Bengal during October–December. *Theoretical and Applied Climatology*, 120(3–4), 797–810. <https://doi.org/10.1007/s00704-014-1214-z>
- Gray, W. M. (1979). Hurricanes: Their formation, structure and likely role in the tropical circulation. D. B. Shaw *Meteorology Over the Tropical Oceans*, 155–218. Bracknell, UK: Royal Meteorological Society.
- Hack, J. J., & Schubert, W. H. (1986). Nonlinear response of atmospheric vortices to heating by organized cumulus convection. *Journal of the Atmospheric Sciences*, 43(15), 1559–1573. [https://doi.org/10.1175/1520-0469\(1986\)043%3C1559:NROAVT%3E2.0.CO;2](https://doi.org/10.1175/1520-0469(1986)043%3C1559:NROAVT%3E2.0.CO;2)
- Ho, C. H., Kim, J. H., Jeong, J. H., Kim, H. S., & Chen, D. (2006). Variation of tropical cyclone activity in the South Indian Ocean: El Niño–southern oscillation and madden-Julian oscillation effects. *Journal of Geophysical Research*, 111, D22101. <https://doi.org/10.1029/2006JD007289>
- Hong, C.-C., Tsou, C.-H., Lee, M.-Y., Chang, C.-C., Hsu, H.-H., & Chen, K.-C. (2018). Effect of ISO-SSE interaction on accelerating the TS to severe TS development in the WNP since the late 1990s. *Geophysical Research Letters*, 45, 12,008–12,014. <https://doi.org/10.1029/2018GL079548>
- Hurrell, J., Meehl, G. A., Bader, D., Delworth, T. L., Kirtman, B., & Wielicki, B. (2009). A unified modeling approach to climate system prediction. *Bulletin of the American Meteorological Society*, 90(12), 1819–1832. <https://doi.org/10.1175/2009BAMS2752.1>
- Kalnay, E., Kanamitsu, M., Kistler, R., Collins, W. D., Deaven, D. G., Gandin, L. S., et al. (1996). The NCEP/NCAR 40-year reanalysis project. *Bulletin of the American Meteorological Society*, 77(3), 437–471. [https://doi.org/10.1175/1520-0477\(1996\)077%3C0437:TNYRP%3E2.0.CO;2](https://doi.org/10.1175/1520-0477(1996)077%3C0437:TNYRP%3E2.0.CO;2)
- Kikuchi, K., Wang, B., & Fudeyasu, H. (2009). Genesis of tropical cyclone Nargis revealed by multiple satellite observations. *Geophysical Research Letters*, 36, L06811. <https://doi.org/10.1029/2009GL037296>
- Krishnamohan, K., Mohanakumar, K., & Joseph, P. (2012). The influence of Madden–Julian oscillation in the genesis of North Indian Ocean tropical cyclones. *Theoretical and Applied Climatology*, 109(1–2), 271–282. <https://doi.org/10.1007/s00704-011-0582-x>
- Lau, K.-H., & Lau, N.-C. (1992). The energetics and propagation dynamics of tropical summertime synoptic-scale disturbances. *Monthly Weather Review*, 120(11), 2523–2539. [https://doi.org/10.1175/1520-0493\(1992\)120%3C2523:TEAPDO%3E2.0.CO;2](https://doi.org/10.1175/1520-0493(1992)120%3C2523:TEAPDO%3E2.0.CO;2)
- Mahala, B. K., Nayak, B. K., & Mohanty, P. K. (2015). Impacts of ENSO and IOD on tropical cyclone activity in the Bay of Bengal. *Natural Hazards*, 75(2), 1105–1125. <https://doi.org/10.1007/s11069-014-1360-8>
- Maloney, E. D., & Dickinson, M. J. (2003). The intraseasonal oscillation and the energetics of summertime tropical western North Pacific synoptic-scale disturbances. *Journal of the Atmospheric Sciences*, 60(17), 2153–2168. [https://doi.org/10.1175/1520-0469\(2003\)060%3C2153:TIOATE%3E2.0.CO;2](https://doi.org/10.1175/1520-0469(2003)060%3C2153:TIOATE%3E2.0.CO;2)
- Maloney, E. D., & Hartmann, D. L. (2001). The Madden–Julian oscillation, Barotropic dynamics, and North Pacific tropical cyclone formation. Part I: Observations. *Journal of the Atmospheric Sciences*, 58(17), 2545–2558. [https://doi.org/10.1175/1520-0469\(2001\)058%3C2545:tmjod%3E2.0.co;2](https://doi.org/10.1175/1520-0469(2001)058%3C2545:tmjod%3E2.0.co;2)
- Ng, E. K. W., & Chan, J. C. L. (2012). Interannual variations of tropical cyclone activity over the North Indian Ocean. *International Journal of Climatology*, 32(6), 819–830. <https://doi.org/10.1002/joc.2304>
- Palmer, T., Doblas-Reyes, F., Weisheimer, A., & Rodwell, M. (2008). Toward seamless prediction: Calibration of climate change projections using seasonal forecasts. *Bulletin of the American Meteorological Society*, 89(4), 459–470. <https://doi.org/10.1175/BAMS-89-4-459>
- Pyper, B. J., & Peterman, R. M. (1998). Comparison of methods to account for autocorrelation in correlation analyses of fish data. *Canadian Journal of Fisheries and Aquatic Sciences*, 55(9), 2127–2140. <https://doi.org/10.1139/f98-104>
- Reynolds, R. W., Smith, T. M., Liu, C., Chelton, D. B., Casey, K. S., & Schlax, M. G. (2007). Daily high-resolution-blended analyses for sea surface temperature. *Journal of Climate*, 20(22), 5473–5496. <https://doi.org/10.1175/2007JCLI1824.1>
- Schade, L. R., & Emanuel, K. A. (1999). The ocean's effect on the intensity of tropical cyclones: Results from a simple coupled atmosphere–ocean model. *Journal of the Atmospheric Sciences*, 56(4), 642–651. [https://doi.org/10.1175/1520-0469\(1999\)056%3C0642:TOSEOT%3E2.0.CO;2](https://doi.org/10.1175/1520-0469(1999)056%3C0642:TOSEOT%3E2.0.CO;2)
- Sobel, A. H., & Maloney, E. D. (2000). Effect of ENSO and the MJO on western North Pacific tropical cyclones. *Geophysical Research Letters*, 27(12), 1739–1742. <https://doi.org/10.1029/1999GL011043>
- Wang, B., & Chan, J. C. L. (2002). How strong ENSO events affect tropical storm activity over the Western North Pacific. *Journal of Climate*, 15(13), 1643–1658. [https://doi.org/10.1175/1520-0442\(2002\)015%3C1643:hseeat%3E2.0.co;2](https://doi.org/10.1175/1520-0442(2002)015%3C1643:hseeat%3E2.0.co;2)
- Webster, P. J. (2008). Myanmar's deadly daffodil. *Nature Geoscience*, 1(8), 488–490. <https://doi.org/10.1038/ngeo257>

- Wheeler, M. C., & Hendon, H. H. (2004). An all-season real-time multivariate MJO index: Development of an index for monitoring and prediction. *Monthly Weather Review*, 132(8), 1917–1932. [https://doi.org/10.1175/1520-0493\(2004\)132%3C1917:AARMMI%3E2.0.CO;2](https://doi.org/10.1175/1520-0493(2004)132%3C1917:AARMMI%3E2.0.CO;2)
- Yuan, J., & Cao, J. (2013). North Indian Ocean tropical cyclone activities influenced by the Indian Ocean dipole mode. *Science China Earth Sciences*, 56(5), 855–865. <https://doi.org/10.1007/s11430-012-4559-0>
- Zehr, R. M. (1992). Tropical Cyclogenesis in the Western North Pacific.
- Zhan, R., Wang, Y., & Lei, X. (2011). Contributions of ENSO and East Indian Ocean SSTAs to the interannual variability of Northwest Pacific tropical cyclone frequency. *Journal of Climate*, 24(2), 509–521. <https://doi.org/10.1175/2010JCLI3808.1>
- Zhang, C. (2005). Madden-Julian oscillation. *Reviews of Geophysics*, 43, RG2003. <https://doi.org/10.1029/2004rg000158>
- Zhang, C. D. (2013). Madden-Julian oscillation bridging weather and climate. *Bulletin of the American Meteorological Society*, 94(12), 1849–1870. <https://doi.org/10.1175/BAMS-D-12-00026.1>
- Zhang, M., Zhou, L., Chen, D., & Wang, C. (2016). A genesis potential index for Western North Pacific tropical cyclones by using oceanic parameters. *Journal of Geophysical Research: Oceans*, 121, 7176–7191. <https://doi.org/10.1002/2016jc011851>
- Zhao, M., & Held, I. M. (2012). TC-permitting GCM simulations of hurricane frequency response to sea surface temperature anomalies projected for the late-twenty-first century. *Journal of Climate*, 25(8), 2995–3009. <https://doi.org/10.1175/jcli-d-11-00313.1>
- Zhou, L., Murtugudde, R., Chen, D., & Tang, Y. M. (2017a). Seasonal and interannual Variabilities of the Central Indian Ocean mode. *Journal of Climate*, 30(16), 6505–6520. <https://doi.org/10.1175/JCLI-D-16-0616.1>
- Zhou, L., Murtugudde, R., Chen, D., & Tang, Y. (2017b). A Central Indian Ocean mode and heavy precipitation during the Indian summer monsoon. *Journal of Climate*, 30(6), 2055–2067. <https://doi.org/10.1175/JCLI-D-16-0347.1>
- Zhou, L., Murtugudde, R., Neale, R. B., & Jochum, M. (2018). Simulation of the Central Indian Ocean mode in CESM: Implications for the Indian summer monsoon system. *Journal of Geophysical Research: Atmospheres*, 123(1), 58–72. <https://doi.org/10.1002/2017JD027171>
- Zhou, L., Sobel, A. H., & Murtugudde, R. (2012). Kinetic energy budget for the madden-Julian oscillation in a multiscale framework. *Journal of Climate*, 25(15), 5386–5403. <https://doi.org/10.1175/JCLI-D-11-00339.1>